

Composite Grid Technology

Applied to VEGA-C Interstage 2/3

A. Zallo (1), Luca Ippati (1), A. Grilli (1), F. De Nicola (2), G. Totaro (2), G. Giusto (2), P. Spena (2), F. Di Caprio (2), S. Mespoulet (3)

(1) Avio s.p.a – Via Ariana Km 5.2 - 00034 Colleferro (Rome), Italy, antonio.zallo@avio.com

(2) CIRA – Via Maiorise 81043 - Capua (CE), Italy, f.denicola@cira.it

(3) ESA - Largo Galileo Galilei 1 – CP 64 - 00044 Frascati (Rome), Italy, Stephane.Mespoulet@esa.int

Abstract

The Interstage 2/3 is the structure that interfaces the Z40 second stage with the Z9 third stage on the VEGA-C launch vehicle. The primary structure is a regular and rather dense network of interlaced hoop and helical unidirectional ribs obtained using a continuous deposition process of carbon fibres followed by epoxy resin infusion. This grid structure is completed with a thin outer carbon skin which has a secondary structural role. The current work presents the production and mechanical testing of the scale one demonstration model. It demonstrates the suitability of the composite grid technology for carrying launcher structures applications.

1. Introduction

The composite grid technology is perfectly suited for applications that require high mass efficiency under significant mechanical in-service loads. Despite this advantage, the grid technology has had very few practical applications to date in load carrying structures for space vehicles. The reason behind this is associated with the low maturity of the manufacturing process, and in particular with the difficulty to ensure a homogeneous material state in the nodal regions. Over the past years, CIRA (Italian Aerospace Research Centre) has worked extensively on the topic and managed to bring the manufacturing process to a level of maturity ready for industrial application. The technology is now applied for the interstage 2/3 by AVIO on the on-going ESA-supported Vega-C development. The maiden flight of Vega-C is planned early 2020.

1.1 Composite Grid Technology

The composite grid technology was developed by CIRA [1]. It is based on the Robotic/Filament Winding of dry carbon fibre tows that are laid down in the grooves of a rubber carpet reproducing the grid pattern. The process is completed with resin infusion under vacuum bag. This process brings the following advantages:

- The dry preform is fully interlaced ensuring optimum load transfer thanks to the patented deposition process [2],
- The mass efficiency is higher than classic manufacturing processes since large surface areas are void of material with ribs taking all the loads,
- The fibre volumetric fraction, the regularity of the cross-section along the rib and across the nodes and the basic mechanical properties are very similar to the wet winding process,
- The dry winding process eliminates the exposure to solvents and volatiles of the resin, avoids pot life problems, and limits the entrapping of air bubbles.

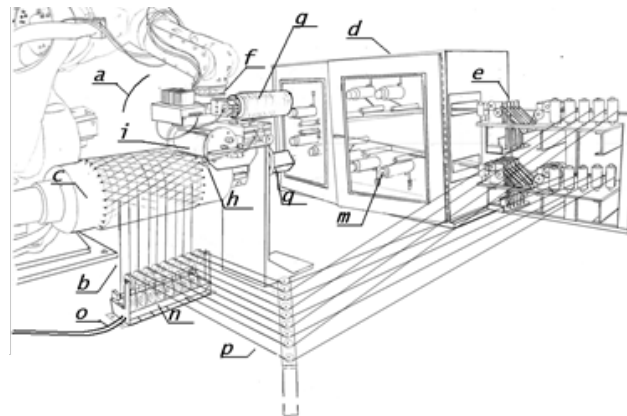


Figure 1: Patented technique to interlace the grid structure ribs (helixes) and hoop

Additionally, CIRA developed analytical optimization methods supported by experimental validation [3] to get the best-suited design for the application.

1.2 Interstage 2/3 Design

The interstage 2/3 is the connecting structure between the second stage (Zefiro 40) and third stage (zefiro 9) of the Vega-C launch vehicle.

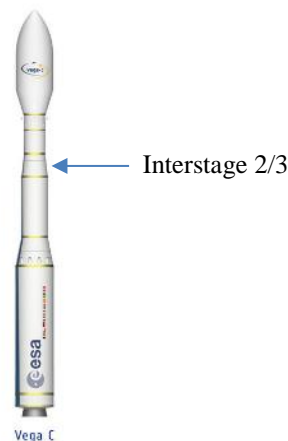


Figure 2: Vega-C Launch Vehicle

Is is designed to fulfil the following main functions:

- F1. To transmit the thrust from the second stage SRM to the launcher third stage,
- F2. To provide a minimum overall stiffness,
- F3. To house (and protect) equipment items and components,
- F4. To guarantee the separation of the second stage.

The requirements stemming from these functions and the design choices implemented on the interstage 2/3 are:

- F1 Sustain high compressive loads, i.e. high buckling capacity. Grid structure is particularly suitable for this failure mode.
- F2 Require high modulus material. Unidirectional carbon fibres.
- F3 Request efficient interface design between structure and equipment brackets. Carried out through inbedded insert design.
- F4 Presence of explosive pyroline fitted in aluminium ring. Interface design between grid structure and aluminium ring (also for top and bottom flanges) ensuring high load transfer capacity (adjusted bolt design).

The final design is a 165 kg carbon grid structure that can sustain an overall compression load of 430 tons. The structure is composed of:

- 120 helixes with rectangular cross section,
- 10 hoops with rectangular cross section,
- Helix angle: 16 to 20°,
- 4 CFRP end rings which allow the connection between the CFRP grid structure and the metallic flanges of the interstage

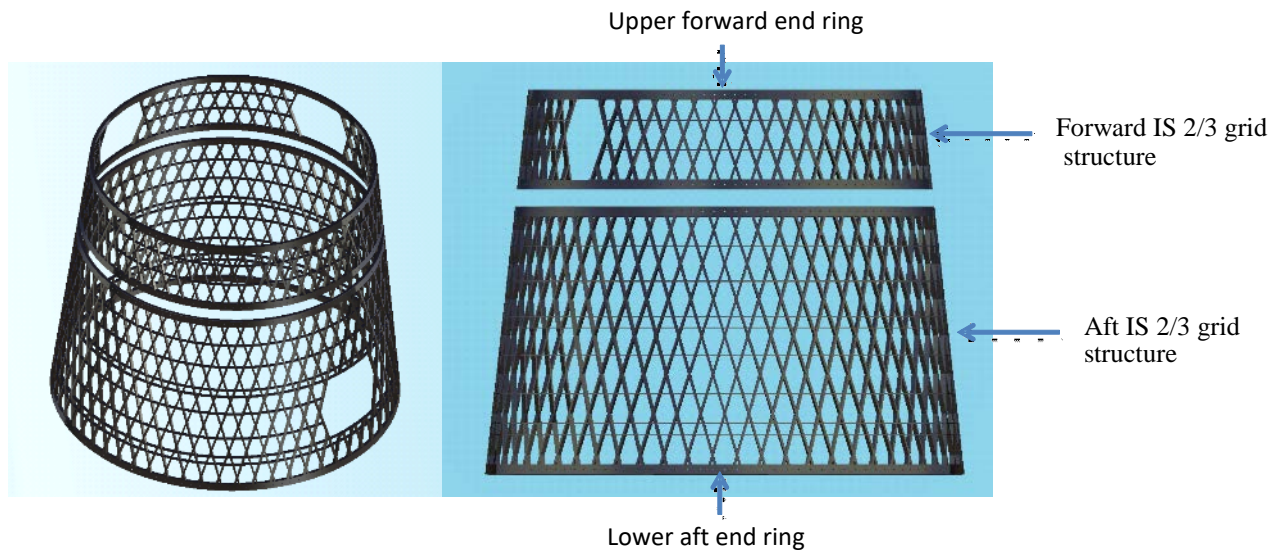


Figure 3: IS 2/3 grid structure layout (the outer skin is not represented)

The forward and aft access door openings are cut out by direct trimming of the ribs. Connections between the metallic flanges and the CFRP end rings are made of close fit shear bolts. Internal equipment items, separation spring supports, access door frames and closure panels are connected to the composite structure through metallic inserts positioned directly in the helixes before winding.

2 Development Model Production

The first scale one model for the interstage 2/3 was produced and tested in 2018. The results from development samples tests was reported in [4]. The current paper focuses on the results from the scale 1 AIT activities carried out on the development model (DM).

2.1 Manufacturing

The main phases of the general manufacturing process for the composite part are:

- Preparation and assembly of the rubber carpet on the mandrel and general set-up
- “Parallel Winding” of the Grid structure, including black rings
- Winding of the outer skin
- Resin infusion at low temperature under vacuum bag and autoclave cure



Figure 4: IS 2/3 composite structure during ribs and helixes winding

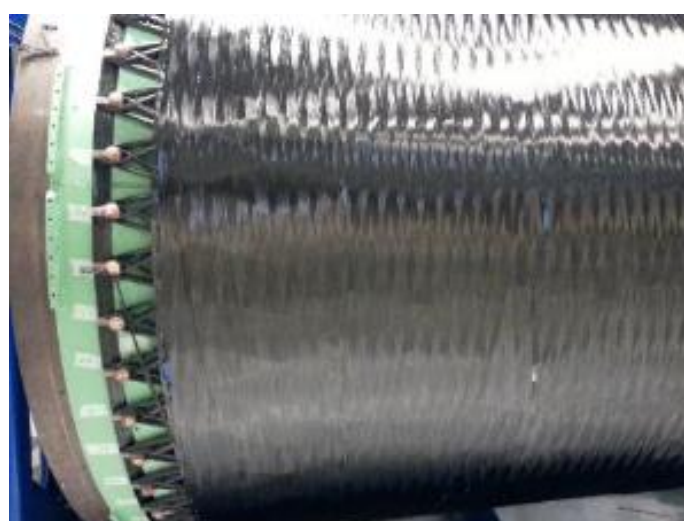


Figure 5: IS 2/3 composite structure during skin winding



Figure 6: IS 2/3 composite structure after cure (inside view)

No major issue occurred during the composite manufacturing. A minor difficulty was linked to the difficulty in removing the structure from the mould. The mould outer surface was then covered with a low friction material, ensuring load-free removal of subsequent productions.

The composite structure was then trimmed and assembled with its aluminium rings and access doors on a dedicated integration stand. The brackets were subsequently mounted on the inner surface through the co-cured inserts.

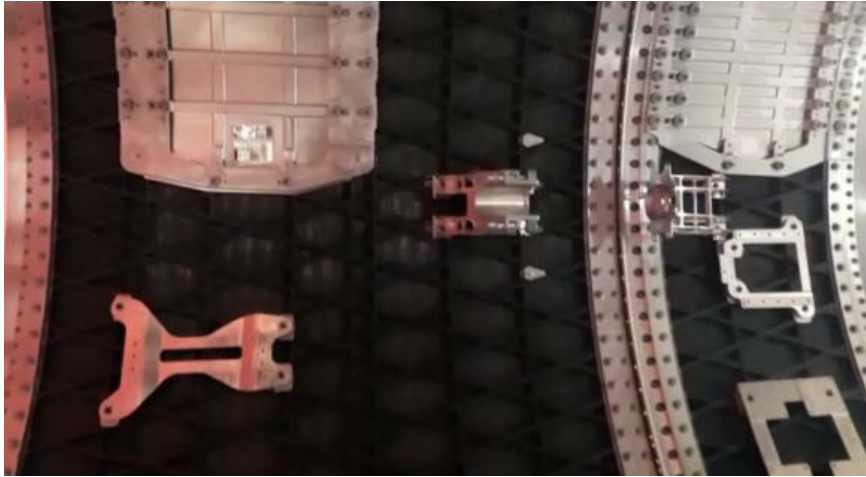


Figure 7: IS 2/3 assembled and equipped structure (inside view)

2.2 Inspection

Both C-scan ultrasonic inspection and X-ray radiography were carried out on the composite structure. No unacceptable defect was detected.



Figure 8: Radiography of IS 2/3 composite structure (partial)

All other dimensional controls were in line with requirements. Mass measurement was compliant with prediction.

3 DM Static Load Test

The objective of the static load test was to:

- Measure axial and bending stiffness
- Demonstrate load carrying capabilities at 100% of maximum induced mechanical flux (aerodynamic and inertial loads combined)

3.1 Configuration

Tension and compression were applied to the DM structure through 6 hydraulic jacks. In order to avoid as much as possible localized over-fluxes, a massive steel handling ring was installed on top of the IS 2/3 forward connection flange.

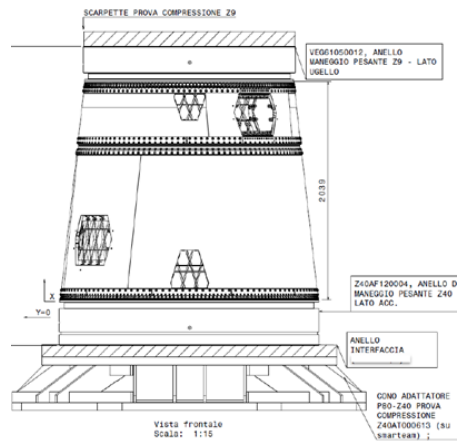


Figure 9: Static load test configuration



Figure 10: Load introduction during static load test –Bottom view of interstage 2-3

The load introduction during the static load test is equivalent to the loading conditions during flight.

Both displacements and strains were measured for a total of 155 measurement channels.

Table 1: Measurement points list

Device	N°	Channels
Potentiometers	6	6
Uni-axial strain gauges	62	62
Tri-axial strain gauges	29	87

Uni-axial strain gages were used in Ribs location with an increase of measurement points in the area around the load carrying doors.

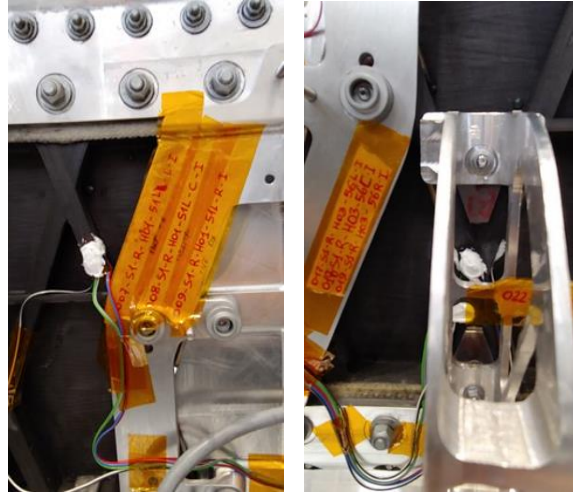


Figure 11: Strain gauges around access door

Due to planning constraints, potentiometers for displacement measurements were only installed on the forward connection flange.

3.2 Stiffness Results

Bending stiffness experimental results showed a measured value equal to 97% of the numerical simulation.

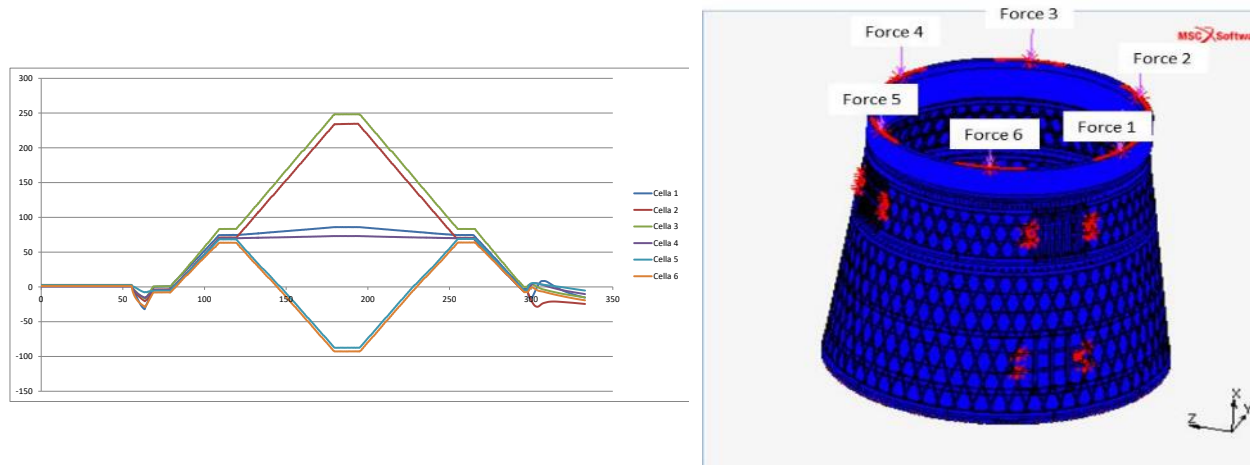


Figure 12: Bending test – Measured applied force for each loading cell [kN] vs time

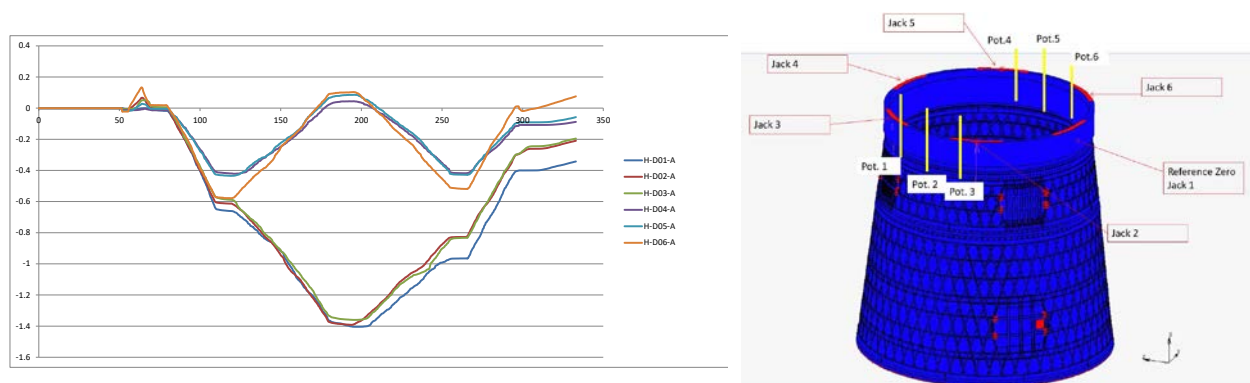


Figure 13: Bending test – Measured resultant displacement [mm] vs time

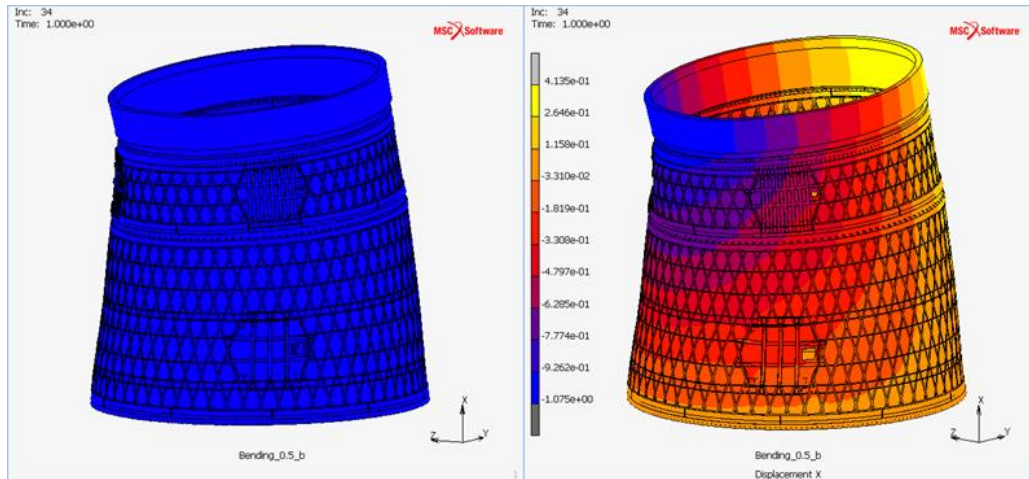


Figure 14: Bending test – predicted axial displacement [mm] due to bending

The measured axial stiffness was about 35% below numerical predictions. Since only displacements on the top flange were measured, this poor correlation could be associated to a test bench stiffness lower than expected due to bolted joint connections. Such effect is not significant for the bending test since the resultant load on the bench is only about 20 tons. This is much lower than the resultant load of 350 tons applied during the compression case. For the qualification model static load test, displacements will be measured also at the lower test bench interface and on all IS 2/3 metallic flanges.

3.3 Strength Results

The strain distribution on the forward flange was in line with the numerical predictions as shown in the figure below in which are also shown the position of the forward (the smaller) and aft (the larger) access doors as well as the position of the hydraulic jacks (orange arrows).

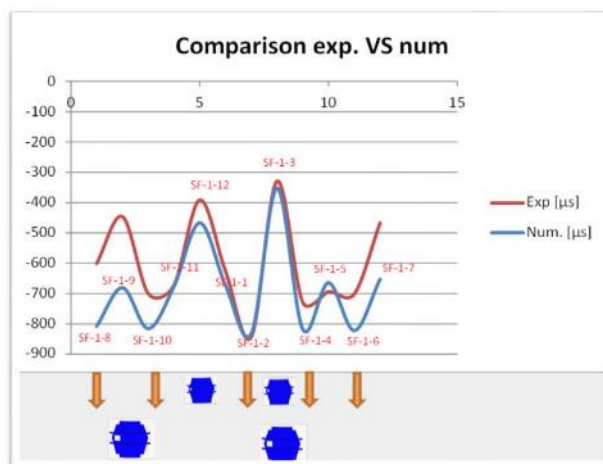


Figure 15: Strain distribution on forward flange

The stress distribution around the closure panels was in line with predictions for the forward door and below expected for the aft access door.

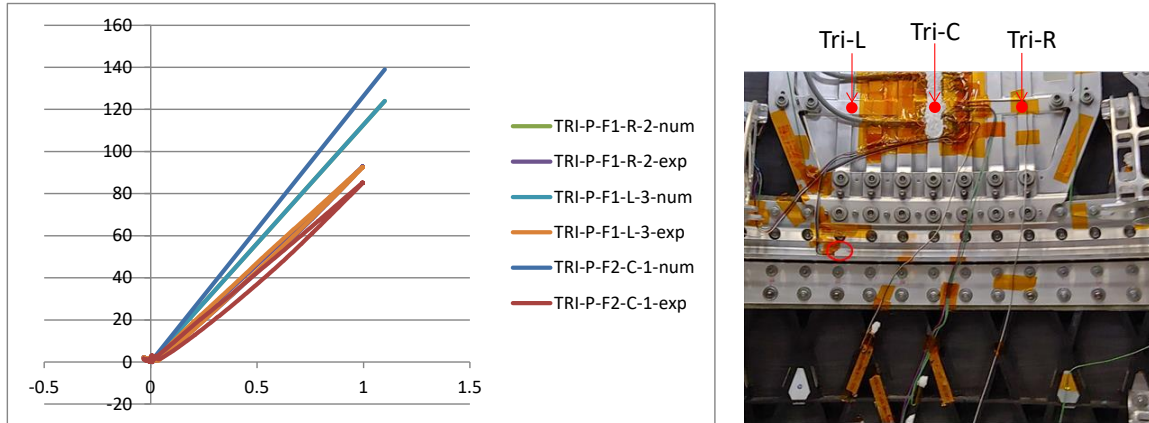


Figure 16: Comparison numerical vs experimental stress distribution on forward closure panel (von Mises)

Table 2: Synthesis of experimental measured stress over numerical predicted ratio in correspondence of access door

	FWD Closure Panel 1			FWD Closure Panel 2		
	TRI-P-F1-C-1	TRI-P-F1-R-2	TRI-P-F1-L-3	TRI-P-F2-C-1	TRI-P-F2-R-2	TRI-P-F2-L-3
Exp./num. ratio	0.68	0.82	0.82	0.67	0.87	0.82
	AFT Closure Panel 1			AFT Closure Panel 2		
	TRI-P-A1-C-1	TRI-P-A1-R-2	TRI-P-A1-L-3	TRI-P-A2-C-1	TRI-P-A2-R-2	TRI-P-A2-L-3
Exp./num. ratio	0.36	0.55	0.64	0.34	0.53	0.67
	FWD Frame 1	FWD Frame 2	AFT Frame 1	AFTFrame 2		
	TRI-F-F1-L-1	TRI-F-F2-L-1	TRI-F-A1-R-2	TRI-F-A2-R-2	TRI-F-A2-L-1	
Exp./num. ratio	1.07	1.16	0.33	0.43	0.33	

The strain distribution on the ribs around both Aft and Forward Closure panels was close to the numerical simulation: the deviation with respect to the prediction is within $\pm 20\%$

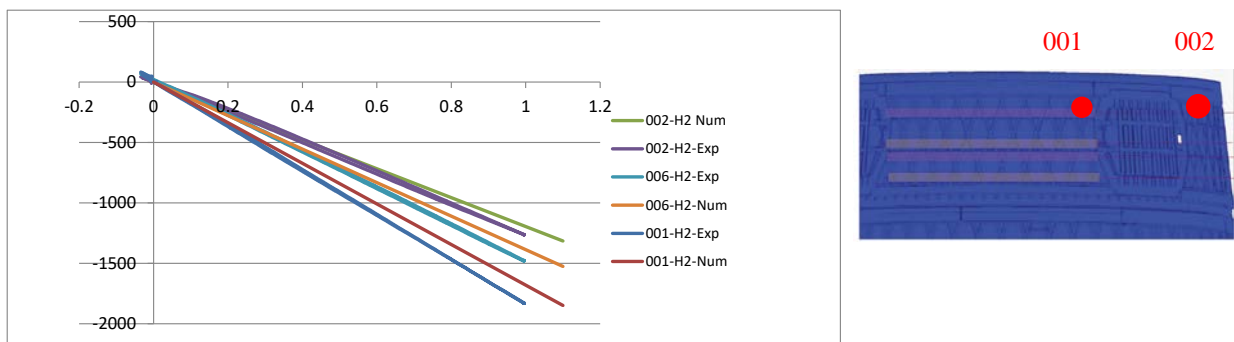


Figure 17: Comparison numerical vs experimental strain distribution in ribs (001, 002 around the forward closure panel; 006 in forward cone away from discontinuities)

Table 3: Synthesis of experimental measured stress over numerical predicted ratio in correspondence of the ribs

Around FWD Access Door		Average on rib section	Around AFT Closure door		FWD Cone		AFT Cone	
001-S1-R-H01-06L-C-I	0.95	-	033-S1-R-H10-21L-C-I	1.08	005-S1-R-H01-22L-C-I	1.15	024-S1-R-H05-08L-C-I	1.15
002-S1-R-H01-11R-L-I	1.05	-	034-S1-R-H10-50L-C-I	1.11	006-S1-R-H01-38R-C-I	1.06	025-S1-R-H06-08R-C-I	1.01
003-S1-R-H01-11R-C-I	1.20	1.17	036-S1-R-H12-21R-C-I	1.00	011-S1-R-H02-21R-C-I	0.97	026-S1-R-H07-08R-C-I	0.84
004-S1-R-H01-11R-R-I	1.26	-	037-S1-R-H12-27L-C-I	1.05	012-S1-R-H02-39L-C-I	0.87	027-S1-R-H07-19L-C-I	1.08
007-S1-R-H01-51L-L-I	0.81	-	039-S1-R-H12-51R-C-I	0.97	016-S1-R-H03-22R-C-I	NA	028-S1-R-H07-39R-C-I	0.90
008-S1-R-H01-51L-C-I	1.15	1.05	040-S1-R-H12-57L-C-I	1.06	021-S1-R-H04-22L-C-I	1.28	029-S1-R-H08-08L-C-I	0.94
009-S1-R-H01-51L-R-I	1.20	-	041-S1-R-H15-21R-C-I	1.02	-	-	030-S1-R-H08-39L-C-I	0.95
010-S1-R-H01-56L-C-I	1.24	-	042-S1-R-H15-27L-C-I	0.91	-	-	031-S1-R-H08-19R-C-I	1.00
013-S1-R-H03-06L-L-I	0.52	-	043-S1-R-H15-51R-C-I	1.12	-	-	032-S1-R-H10-07R-C-I	0.99
014-S1-R-H03-06L-C-I	0.76	0.82	044-S1-R-H15-57L-C-I	0.97	-	-	035-S1-R-H12-08L-C-I	0.28
015-S1-R-H03-06L-R-I	1.17	-	045-S1-R-H17-24L-C-I	1.13	-	-	038-S1-R-H12-37L-C-I	0.96
017-S1-R-H03-56L-L-I	1.19	-	046-S1-R-H17-24R-C-I	1.14	-	-	-	-
018-S1-R-H03-56L-C-I	1.24	1.20	047-S1-R-H17-27R-C-I	1.08	-	-	-	-
019-S1-R-H03-56L-R-I	1.18	-	048-S1-R-H17-54L-C-I	1.06	-	-	-	-
022-S1-R-H04-57L-C-I	1.05	-	049-S1-R-H17-54R-C-I	0.91	-	-	-	-
023-S1-R-H04-12L-C-I	1.46	-	050-S1-R-H17-57R-C-I	0.98	-	-	-	-
Total Average ratio exp/num.		1.09	Total Average ratio exp/num.	1.05	Total Average ratio exp/num.	1.07	Total Average ratio exp/num.	0.92

4 DM Shock Test

4.1 Configuration

The configuration tested was fully representative of the flight configuration. Equipment dummy masses were installed at the exact locations of the flight items. The IS 2/3 was also equipped with 8 separation springs plus the guiding system for supporting the separation kinematic.

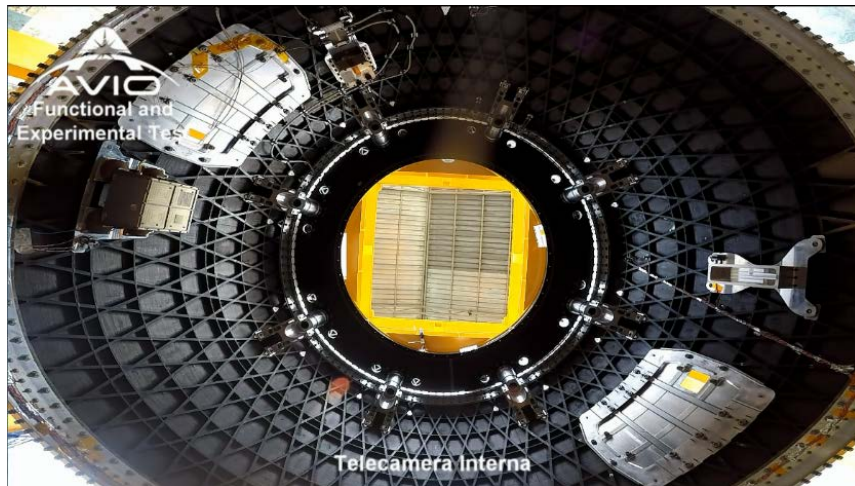


Figure 18: camera view of internal interstage volume before firing

4.2 Results

Analysis of high speed camera has shown very good kinematic behaviour. The guiding system has ensured a very straight translation of the aft cone after cutting charge activation (under gravity conditions).

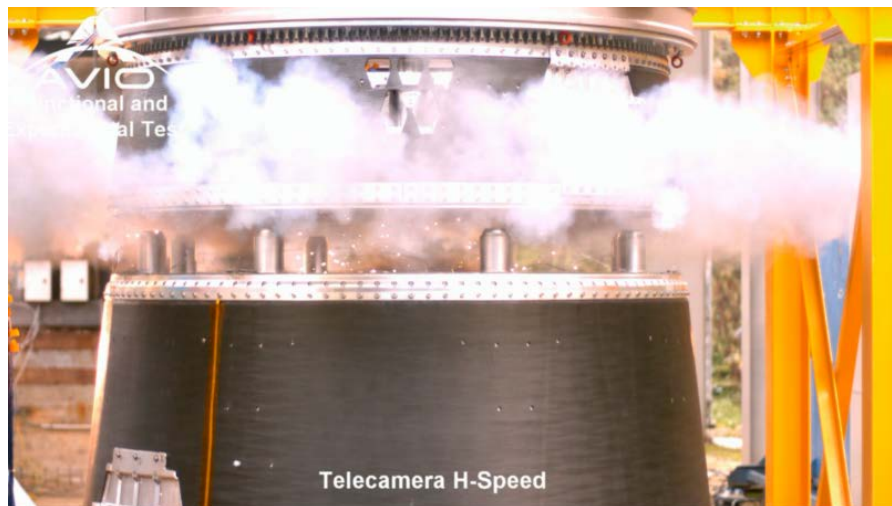


Figure 19: High speed camera screen-shot

Accelerations were measured in several points inside the IS 2/3 in order to have the induced shock levels at significant interfaces.

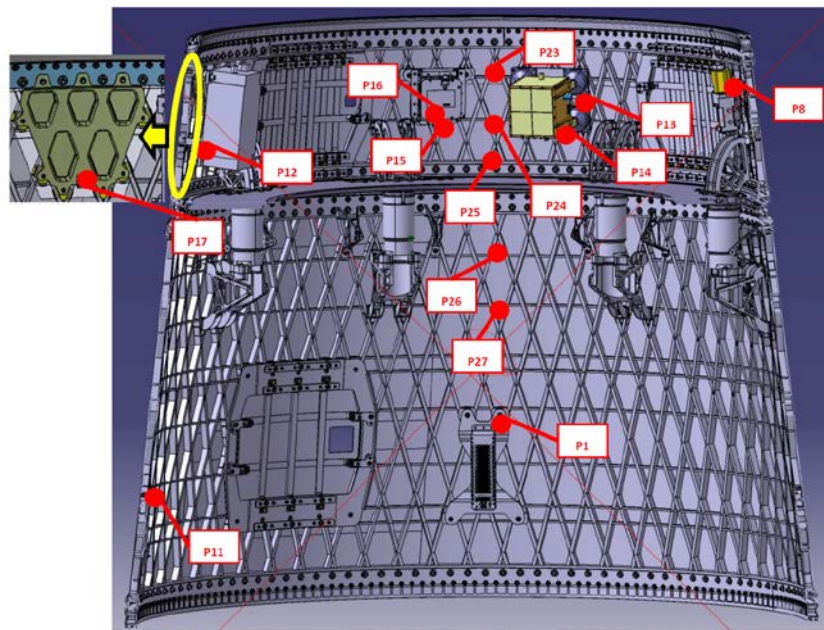


Figure 20: Accelerometers layout during DM shock test

The shock levels measured at the base of the equipments were all below specification.

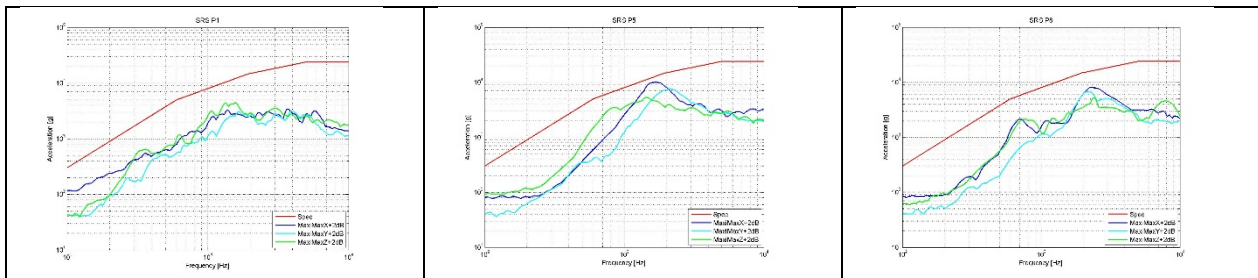


Figure 21: Examples of shock response spectra obtained during the DM shock test

The measured shock levels on the DM were lower than the shock levels at the equivalent locations on the classic metallic IS 2/3 although the separation system has not been modified in terms of linear explosive charge and cross-section to cut. This lower transmissibility to the equipments installed on the structure is due to the composite grid design and to the connection of the equipment supports to the ribs. This connection is made of co-cured metallic inserts. Load is transmitted from the ribs to the metallic inserts through shearing at the insert/rib interfaces. Since the ribs are much stiffer than the metallic inserts, the shock is primarily transmitted in the grid. The small portion of the shock that is transmitted to the equipment is attenuated thanks to the large rib /insert interface.

5 Upcoming Activities

5.1 QM Static Load Test

The manufacturing and inspection of the qualification model (QM) model are in progress. It is planned to have the QM ready for test at the beginning of July 2019. Static bending, compression and tension loading conditions will be applied with a safety factor equal to 1.25 (qualification level). After X-ray inspection at the end of the ultimate run, the structure will be brought to collapse on the dimensioning load case.

5.2 Qualification Activities

Apart from the static load test campaign, other qualification activities are planned before the qualification review can be held:

- Test in relevant dynamic environment to demonstrate reliability of joints between equipment support and grid structure. This test will also characterise the structural damping of this type of technology. The test is planned in July 2019;
- Access door closure panel installation test. This test aims at demonstrating the feasibility to mount the load carrying access door when the IS 2/3 is supporting the upper part of the launcher. In case mountability is not demonstrated or is marginal, limited and already identified design modifications will be implemented and tested.
- Ageing of CFRP components to identify knock down factor due to water absorption;
- Qualification of metallic parts manufacturing processes including material ageing and surface coating application
- Qualification of bonding processes (mainly external thermal protection bonding on external IS 2/3 surface);

6 Conclusion

The static load test of the first grid technology scale one model has been performed successfully. The capacity of the IS 2/3 structure to comply with stringent stiffness requirements and sustain flight loads has been demonstrated. The numerical models predict with acceptable accuracy the behaviour of the structure. The design and manufacturing processes are now validated. In addition, the grid technology associated with the retained inserts design ensure better protection against shock from the stage separation for the equipments mounted on the IS 2/3 when compared to classic structures.

The DM production and test campaign has cleared the way for the qualification of the IS 2/3 planned before end 2019. With the maiden flight planned early 2020, the composite grid technology will move from laboratory to a demanding operational application.

7 References

- [1] G. Totaro, F. De Nicola, "Recent advance on design and manufacturing of composite anisogrid structures for space launchers", *Acta Astronautica* 81:570-577, 2012.
- [2] F. De Nicola, G. Totaro, C. Vitiello, "Sistema per la Deposizione di materiali compositi in Wet Winding con rotazione infinita dell'occhio e con distribuzione parallela di supporto", Patent IT0001397218.
- [3] G. Totaro, Z. Gurdal, "Optimal design of composite lattice shell structures for aerospace applications", *Aerospace Science and Technology*. Vol 13, Issues 4-5, June-July 2009, pages 157-164
- [4] A. Zallo, A. Grilli, F. De Nicola, G. Totaro, G. Giusto, P. Spena, F. Di Caprio, S. Mespoulet, "General overview of grid technology design for Vega-C interstage 2/3", 15th European Conference on Spacecraft Structures, Materials and Environmental Testing (ECSSMET 2018), Noordwijk, 2018.